J|A|C|S
COMMUNICATIONS

Published on Web 11/16/2006

Preparation of Multilayered Trimodal Colloid Crystals and Binary Inverse Opals

Jianjun Wang, Qin Li, Wolfgang Knoll, and Ulrich Jonas*

Max Planck Institute for Polymer Research, Ackermannweg 10, 55128 Mainz, Germany

Received October 13, 2006; E-mail: jonas@mpip-mainz.mpg.de

The quest for photonic materials has reanimated colloidal crystal research with an emergence of innovative preparation methods, new ordered structures, and applications. Colloidal crystal self-assembly has attracted particular attention due to its potential as an efficient, inexpensive mass production method.[1] In addition, it provides the possibility to prepare ordered states of matter that are not accessible by other existing nanofabrication methods.[2] The self-assembly process involving multiple colloidal components of different materials and dimensions offers additional potential. For example, multicomponent colloidal crystals can provide intricate structures as the basis for photonic and phononic band gap materials and multiscale porous materials with very large surface area for applications in ion exchange, molecular separation, catalysis, chromatography, biomaterials engineering, and membrane reactors.[3]

Recent work has been directed toward the preparation and characterization of binary colloidal crystals.[4] This study reports the first successful co-transfer of a three-component mixture with colloidal particles of different materials and diameters in suspension yielding multilayered trimodal colloid crystals by vertical lifting deposition. Pyrolysis of the organic components in these films led to binary inverse opals with a combination of meso- and macroporous cavities. The optical properties of the prepared materials were characterized by vis−NIR spectroscopy, and the measured spectral shifts allowed quantitative calculation of the volume fraction of all components in the film. The crystal structure deduced from these calculations was compared with computer models of the possible particle packing and agreed well with the morphology observed by SEM.

Scheme 1 illustrates the preparation procedure for the trimodal colloid crystals and their corresponding binary inverse opals. We selected polystyrene (PS) microspheres of a diameter $D = 465$ nm as the large particles, poly(methyl methacrylate) (PMMA) nanospheres $D = 84$ nm as the intermediate colloids, and silica nanoparticles $D = 6$ nm as the small component. The relative size ratios were $\gamma_{I/L} = D_{Intermediate}/D_{Large} = 0.18$, and $\gamma_{S/I} = D_{Small}/D_{Intermediate} = 0.071$, while the relative concentrations were $\phi_{I/L} = C_{Intermediate}/C_{Large} = 0.09$ and $\phi_{S/I} = C_{Small}/C_{Intermediate} = 1.1$. The trimodal films prepared with these parameters maintained the fcc packing of the large PS particles with the intermediate PMMA particles occupying the interstitial voids, while the remaining volume was completely filled with the small silica nanoparticles. These silica particles formed the binary inverse opals after pyrolysis.[5] Apparently, the combined effects of the capillary forces and the liquid flux from the suspension to the drying crystal film drive the trimodal crystallization of the particles into an optimal packing, when the meniscus sweeps over the glass substrate while being lifted from the suspension at a controlled speed. By changing the experimental parameters, the overall film thickness can be varied from 500 nm up to 6 μm.

Figure 1 shows SEM images of the various samples prepared, with the top view of a binary colloidal structure (bCC) consisting

Scheme 1

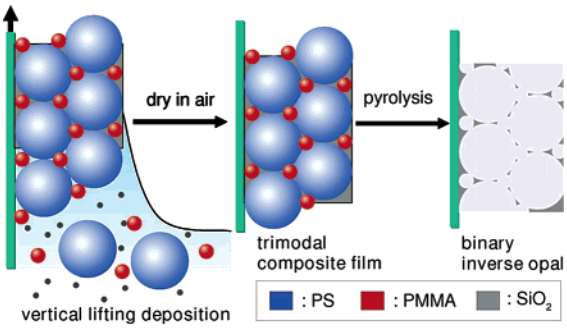

of PS (large) and PMMA (intermediate) in Figure 1a. The 3-fold hollow sites at the (111) surface of the fcc PS crystal are mainly filled with PMMA particle triplets. Because the PMMA particles start to decompose under the electron beam, these triplets show some deformation compared with a stable PS/PS composite crystal.[5]

The image in Figure 1b displays the trimodal PS/PMMA/silica composite film (tCC) which was transferred from a mixed particle suspension with the same PS and PMMA concentration as in Figure 1a and the above specified amount of silica nanoparticles added. In this case, the silica nanoparticles fully occupy the remaining space between the PS and PMMA spheres, with the latter showing beginning decomposition under the electron beam of the microscope. These experiments clearly demonstrate that even in these trimodal particle mixtures the large PS spheres can form a perfect fcc lattice during vertical lifting deposition and accommodate smaller particles in the interstitial space. Figure 1c exhibits the top view of the binary inverse opal (bIO) formed by pyrolysis of the

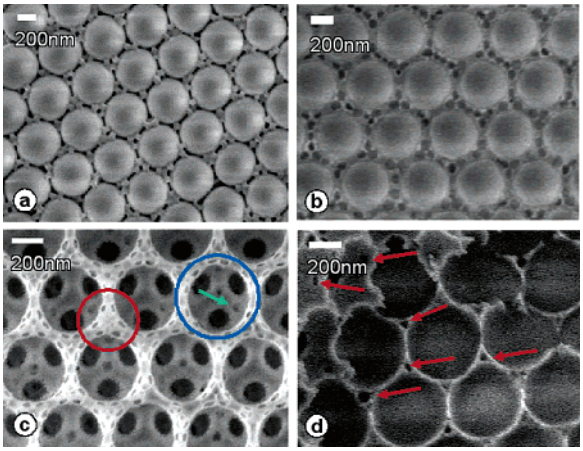

Figure 1. LV-SEM images of the colloid structures. (a) Binary colloid crystal (bCC) from large PS and small PMMA particles. (b) Trimodal CC from large PS, intermediate PMMA, and small silica particles. (c) Top view of binary inverse opal (bIO) after PS and PMMA pyrolysis of the tCC from (b). (d) Fracture of the bIO from (c).

10.1021/ja067221a CCC: $33.50

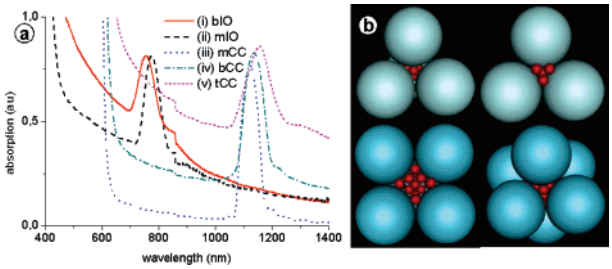

Figure 2. (a) Vis−NIR spectra of the formed binary inverse opal (bIO), monomodal inverse opal (mIO), monomodal colloid crystal (mCC), binary colloidal crystal (bCC), and trimodal colloidal crystal (tCC). (b) Computer simulated filling of the tetrahedral (upper row) and octahedral site (lower row) with small particles ($\gamma = 0.18$).

PS and PMMA particles from the tCC of Figure 1b, leaving a granular silica matrix from the sintered nanoparticles (as indicated by TEM; see Supporting Information, Figure S1b). The sintering process is accompanied with a minor shrinkage of the lattice structure by 2−5%. Highlighted with the blue circle is the first order macropore with a diameter of 456 nm which originates from the large PS particles and is interconnected with 12 neighboring air spheres by the dark 140 nm windows. The highlighted air sphere triplet in the red circle represents the secondary order pores with a dimension of 80 nm, originating from the intermediate PMMA particles. These pores are also connected with each other by small windows that are formed by the particle−particle contact during drying. Since the size of the connecting windows scales with the particle diameter, we estimate the small window diameters between the secondary pores to be about 25 nm in the mesoporous range (80:25 = 456:140). Thus a regular lattice with a hierarchical film structure of interconnected meso- and macropores is easily created by the presented method. The distribution of PMMA particles within the whole composite film (and not only at the surface) is revealed by the black pores marked with the green arrow in Figure 1c and corroborated by the pores (highlighted with the red arrows) in the fractured sample of Figure 1d.

The optical properties of all films were characterized by vis−NIR spectroscopy with the incident light normal to the fcc (111) plane (substrate surface). The spectra are presented in Figure 2a, where the distinct stop band for each structure confirms the high order with a characteristic lattice dimension, despite the coexistence of multiple materials with different length scales. The mCC spectrum (iii) with a peak wavelength of 1122 nm represents the reference for the following discussion. Compared to the mCC, the position of the bCC stop band (iv) shifted to a higher wavelength of 1138 nm, and that of the tCC (v) shifted even higher to 1158 nm. The stop bands of both inverse opals shifted to significantly lower wavelengths, namely, 776 nm (ii) for the monomodal inverse opal (mIO) and 755 nm (i) for bIO.

These stop band shifts can be explained by Bragg's law considering the components' refractive indices and their volume filling fractions.[6] In the case of the bCC, which comprises large PS particles ($n_{PS} = 1.59$) and intermediate PMMA particles ($n_{PMMA} = 1.49$) with air ($n_{air} = 1$) filling the voids, the PS particles pack in a regular fcc lattice with a volume fraction of 0.74. Using Bragg's law (eqs 1 and 2 in Supporting Information) with the measured stop band wavelength of 1138 nm of the bCC, the PMMA volume fraction, ϕ_{PMMA}, was calculated as 9 ± 3%. From the mIO stop band position, a refractive index for the nanoporous silica matrix could be determined as $n_{SilicaMatrix} = 1.19$ (for details, see Supporting Information); ϕ_{PMMA} and ϕ_{PS} in the tCC were regarded as identical to its corresponding bCC since silica nanoparticles do not appear to obstruct the packing manner of larger spheres as shown by SEM.[5] This assumption was confirmed by back calculation of the theoretical tCC and bIO stop band positions. The derived value for ϕ_{PMMA} was further translated into a crystal structure of the bCC, tCC, and bIO, with each large PS particle (L) correlating to approximately 21−23 intermediate (I) PMMA particles. By computer modeling based on geometrical analyses and optimum position searching, it was found for a size ratio of $\gamma_{PMMA/PS} = 0.18$ that each tetrahedral site between four large PS colloids accommodates four intermediate PMMA particles, while each octahedral site (between six PS spheres) can accommodate up to 15 PMMA particles. Results are shown in Figure 2b for PS in blue and PMMA in red (upper left, tetrahedral site viewed from bottom; upper right, an open tetrahedral site with top large particle removed; lower left, an open octahedral site with one large particle removed; lower right, octahedral site viewed from top; see details in Supporting Information). Considering each large sphere is surrounded by eight tetrahedral and six octahedral sites, the stoichiometric composition was derived as LI_{23}. As such, the computer model results correspond well to the ϕ_{PMMA} value deduced from spectral data analysis.

In conclusion, we have prepared multilayered trimodal colloidal structures in a single transfer step using the vertical lifting deposition method. Subsequent pyrolysis led to binary inverse opals. Vis−NIR spectroscopic characterization demonstrated the existence of highly ordered crystal structures. From the spectral data, the volume fraction of the intermediate particles was derived and further translated into an average crystal stoichiometry of LI_{21-23}, which was confirmed by a computer model. Due to the broad adjustable range of particle sizes and size ratios (further details in Supporting Information) as well as the simplicity of the preparation method, this type of hierarchical material offers significant potential in photonics, phononics, separations, and catalysis, to name only a few.

Acknowledgment. Q.L. is thankful for the financial support under the Marie Curie Incoming International Fellowship FP6-022360. This work was partially supported by the BMBF, project FKZ 0312015B.

Supporting Information Available: Detailed information on experimental procedures, computer models, and theoretical calculations. This material is available free of charge via the Internet at http://pubs.acs.org.

References

(1) (a) Norris, D. J.; Arlinghaus, E. G.; Meng, L. L.; Heiny, R.; Scriven, L. E. *Adv. Mater.* **2004**, *16*, 1393−1399. (b) Glotzer, S. C.; Solomon, M. J.; Kotov, N. A. *AIChE J.* **2004**, *50*, 2978−2985. (c) Dutta, J.; Hofmann, H. *Encyclopedia of Nanoscience and Nanotechnology*; Nalwa, H. S., Ed.; American Scientific Publishers: Stevenson Ranch, CA, 2004; Vol. 9, pp 617−639.

(2) (a) Gates, B. D.; Xu, Q.; Stewart, M.; Ryan, D.; Willson, C. G.; Whiteside, G. M. *Chem. Rev.* **2005**, *105*, 1171−1196. (b) Geissler, M.; Xia, Y. N. *Adv. Mater.* **2004**, *16*, 1249−1269.

(3) (a) Joannopoulos, J. D.; Villeneuve, P. R.; Fan, S. *Nature* **1997**, *386*, 143−149. (b) Cheng, W.; Wang, J.; Jonas, U.; Fytas, G.; Stefanou, N. *Nat. Mater.* **2006**, *5*, 830−836. (c) Yang, P.; Deng, T.; Zhao, D.; Feng, P.; Pine, D.; Chmelka, B. F.; Whitesides, G. M.; Stucky, G. D. *Science* **1998**, *282*, 2244−2246. (d) Yuan, Z.; Su, B. *J. Mater. Chem.* **2006**, *16*, 663−677.

(4) (a) Bartlett, P.; Ottewill, R. H.; Pusey, P. N. *Phys. Rev. Lett.* **1992**, *68*, 3801−3804. (b) Leunissen, M. E.; Christova, C. G.; Hynninen, A.-P.; Royall, C. P.; Campell, A. I.; Imhof, A.; Dijkstra, M.; van Roij, R.; van Blaaderen, A. *Nature* **2005**, *437*, 235−240. (c) Kitaev, V.; Ozin, G. A. *Adv. Mater.* **2003**, *15*, 75−78. (d) Wang, D.; Moehwald, H. *Adv. Mater.* **2004**, *16*, 244−247. (e) Bartlett, P.; Campell, A. I. *Phys. Rev. Lett.* **2005**, *95*, 128302-1−4. (f) Velikov, K. P.; Christova, C. G.; Dullens, R. P. A.; van Blaaderen, A. *Science* **2002**, *296*, 106−109.

(5) Wang, J.; Glasser, G.; Neumann, T.; Burkert, K.; Li, Q.; Knoll, W.; Jonas, U. *Adv. Mater.* Submitted for publication.

(6) Miguez, H.; Lopez, C.; Meseguer, F.; Blanco, A.; Vazquez, L.; Mayoral, R.; Ocana, M.; Fornes, V.; Mifsud, A. *Appl. Phys. Lett.* **1997**, *71*, 1148−1150.

JA067221A